Journal of Sound and Vibration (2001) **242**(4), 597–617
doi:10.1006/jsvi.2000.3382, available online at http://www.idealibrary.com on IDEAL®

ON THE BEHAVIOUR OF FLUID-LOADED SANDWICH PANELS WITH MEAN FLOW

N. PEAKE

Department of Applied Mathematics and Theoretical Physics, University of Cambridge, Silver Street, Cambridge CB3 9EW, England. E-mail: n.peake@damtp.cam.ac.uk

AND

S. V. SOROKIN

Department of Engineering Mechanics, St Petersburg State Marine Technical University, 3 Lotsmanskaya str., St Petersburg 190008, *Russia*

(*Received* 25 *November* 1999, *and in final form* 17 *August* 2000)

This paper considers a fluid-loaded sandwich panel, made up of layers of relatively rigid skin material surrounding a layer of less dense core material, with an unsteady point driver in steady mean flow. For a simple plate Brazier-Smith and Scott, and Crighton and Oswell predicted a number of unusual phenomena, including absolute instability, a neutral mode with its group velocity pointing towards the driver, and negative energy waves. The possible occurrence of these phenomena for realistic parameter values is considered. It is shown that absolute instability is unlikely to be found at normal speeds, but in contrast the anomalous propagation mode is present, although over a limited frequency range. It is shown that the negative energy waves could also well occur in practice. Study of both the full dispersion relation and asymptotic analysis demonstrate that at very low frequencies it is the ratio of core to skin stiffnesses and the flow speed which control the dynamics, but at higher frequencies shear coupling and rotational effects become important as well. Consideration of the relative magnitudes of the energy fluxes leads to the unexpected conclusion that for predominantly shear waves more energy is carried in the fluid than is carried in the plate.

1. INTRODUCTION

There is considerable interest in the use of sandwich panels in naval engineering. Such panels usually consist of layers of relatively rigid skin material surrounding layers of less dense core material, and are much lighter than conventional homogeneous plates. A range of theories describing the dynamical behaviour of such sandwich panels have been developed—see, for instance, references, [1–4]. However, their interaction with the surrounding fluid, which in the underwater context is potentially very significant, seems to have received rather little attention to date, and the aim here is to develop the sort of theory previously applied to simple structures (see, for instance, reference [5]) to sandwich panels. In a companion paper, the problem of fluid loading of a sandwich panel in still fluid [6] is described, but here the case in which the fluid has a non-zero mean flow speed is considered. The aim of the analysis is to determine the causal behaviour of such a system driven by a point excitation, by using the Briggs–Bers [7, 8] technique for finding the long-time limit of the solution of initial-value problems. Previous work for a simple plate in uniform mean flow by Brazier-Smith and Scott [9] and by Crighton and Oswell [10] has predicted

0022-460X/01/190597 + 21 $35.00/0

a number of unusual phenomena *which do not arise for zero mean flow*, including absolute instability at sufficiently high normalized flow speed U, a neutral mode with its group velocity pointing towards the driver, and negative energy waves.

The most important difference between a sandwich panel and a simple plate is that as well as the tranverse deflection, in-plane shear motions are also permitted. The approach here is to adopt the model developed by Skvortsov [11, 12], in which high order effects likely to arise when disturbance wave-lengths become comparable to the thicknesses of the sandwich layers are ignored, thereby reducing the motion of the panel to two degrees of freedom, namely a transverse, flexural deflection w and a shear angle θ. The resulting system of equations leads to a dispersion relation which is essentially a seventh order polynomial in the spatial wavenumber (compared to fifth order for the sample plate with mean flow). Four additional dimensionless material parameters are also introduced, measuring the ratios of the core and skin stiffnesses, the strength of coupling between longitudinal shear and transverse flexural motions, and rotational terms in the core and skin.

The model and typical material parameter values are described in section 2. In section 3, it is shown that although absolute instability is theoretically possible over a range of parameter values, it is unlikely to be found in practical situations at normal speeds. In contrast, it is shown in section 4 that the anomalous propagation mode is present for realistic parameter values, but only over a small range of very low driver frequencies. However, in section 5 it is shown that the negative energy waves are likely to be an important practical feature of the dynamics of a sandwich panel, with the effect that the point driver can even act to *remove* energy from the system. The energy fluxes in the fluid and the plate are also considered; for predominantly transverse waves the energy flux in the plate is larger, but for predominantly shear waves it is, surprisingly, the fluid energy flux which dominates.

The analysis here is completed via study of both the full dispersion relation and asymptotic analysis in the realistic limit of small U. This sheds light on a number of issues, such as: the modal structure of the problem, including the existence of two families of modes, one corresponding to predominantly flexural motion and a second to predominantly shear motion; the strength of coupling between the driver and the flexural and shear modes; and the nature of the energy fluxes associated with each of the modes. It turns out that at low frequencies it is the ratio of core to skin stiffnesses and U which control the dynamics, but at higher frequencies shear coupling and rotational effects become important as well.

2. PROBLEM FORMULATION AND SOLUTION

In this section, the system is described in detail, the governing equations are presented and their formal solution derived. The method for determining the long-time limiting behaviour of this solution, which will be the principal concern in this paper, will also be described, and the relevant values of certain important material and flow parameters determined.

2.1. GOVERNING EQUATIONS

Consider the situation shown in Figure 1, in which a sandwich panel lies along the x-axis, with a vacuum in $y < 0$ and with fluid in $y > 0$. The fluid has a mean flow speed U_s in the positive x direction, and the panel is forced to vibrate by an unsteady point driver located at

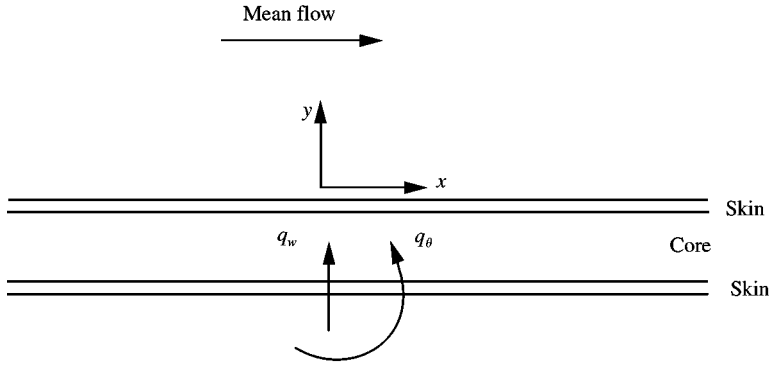

Figure 1. The sandwich panel with mean flow, driven by a point force q_w and point couple q_θ at $x = 0$.

the origin, which generates a force $q_w(t)\,\delta(x)$ and a turning moment $q_\theta(t)\,\delta(x)$. It is supposed that the driver is turned on at time $t = 0$, so that $q_{w,\theta}(t) = 0$ for $t < 0$.

The model used to describe the sandwich panel has been developed by Skvortsov [11, 12], and is equivalent to an extension of Mindlin thick plate theory. The sandwich panel consists of two relatively rigid skin panels and a relatively soft core panel, of thickness $h_{a,b}$, density $\rho_{a,b}$, and Young's moduli $E_{a,b}$ in the longitudinal direction and $G_{a,b}$ in the transverse direction, respectively, and for simplicity, the ratios

$$\varepsilon = h_a/h_b, \quad \delta = \rho_b/\rho_a, \quad \gamma = E_b/E_a, \quad g = G_b/G_a \tag{1}$$

are introduced. The motion of the sandwich panel can be described in terms of transverse, flexural deflection $w(x, t)$ into and out of the fluid, and angle $\theta(x, t)$ corresponding to longitudinal shear deformation, and it is shown in reference [6] that the equations of motion are

$$D_1 \frac{\partial^4 w}{\partial x^4} - \Gamma\left(\frac{\partial\theta}{\partial x} + \frac{\partial^2 w}{\partial x^2}\right) + m\frac{\partial^2 w}{\partial t^2} - I_1 \frac{\partial^4 w}{\partial x^2\,\partial t^2} = q_w(t)\,\delta(x) - p(x, 0, t), \tag{2}$$

$$-D_2 \frac{\partial^2\theta}{\partial x^2} + \Gamma\left(\theta + \frac{\partial w}{\partial x}\right) + I_2 \frac{\partial^2\theta}{\partial t^2} = q_\theta(t)\,\delta(x). \tag{3}$$

Here,

$$m = \rho_a h_a\,[2 + \delta/\varepsilon] \tag{4}$$

is the panel mass per unit area, and

$$D_1 = \frac{E_a h_a^3}{12(1-\nu^2)}\left[2 + \frac{\gamma}{\varepsilon^3}\right], \qquad D_2 = \frac{E_a h_a^3}{2(1-\nu^2)}\left(1 + \frac{1}{\varepsilon}\right)^2, \tag{5, 6}$$

are the effective stiffnesses to flexural and shear motion, with ν the Poisson ratio. In this paper, the Poisson ratios in each material are assumed equal, which is the case for the materials used in the study by Nilsson [4]. However, this restriction is in no way necessary for this theory, and alternative expressions for the various coefficients listed here, with the Poisson ratios unequal and indeed with arbitrarily many plies, can easily be derived.

Further

$$I_1 = \frac{\rho_a h_a^3}{12}\left[2 + \frac{\delta}{\varepsilon^3}\right], \qquad I_2 = \frac{\rho_a h_a^3}{2}\left(1 + \frac{1}{\varepsilon}\right)^2, \tag{7, 8}$$

are the effective moments of inertia of the skin and the core; and

$$\Gamma = \frac{E_a h_a}{2(1-\nu)} \frac{(1 + (1/\varepsilon))^2\, g\varepsilon}{1 + 2g\varepsilon} \tag{9}$$

is a term which describes the coupling between the flexural and shear motions. The term $-p(x, 0, t)$ on the right-hand side of equation (2) corresponds to the loading on the structure from the hydrodynamic pressure in the fluid. This pressure is given by the linearized Bernoulli equation

$$p = -\rho_0\,((\partial\phi/\partial t) + U_s\,(\partial\phi/\partial x)), \tag{10}$$

where ρ_0 is the undisturbed density of the fluid. For the present purposes it is quite sufficient to assume that the fluid is incompressible, so that the velocity potential $\phi(x, y, t)$ satisfies Laplace's equation $\nabla^2\phi = 0$. The motions of the fluid and plate are also coupled together by the normal-velocity boundary condition

$$\partial\phi/\partial y = (\partial w/\partial t) + U_s\,(\partial w/\partial x) \quad \text{on } y = 0. \tag{11}$$

In order to be able to compare the results with the Crighton and Oswell work [10], the problem is now non-dimensionalized by using their length scale m/ρ_0 and their time scale $m^{5/2}/D_1^{1/2}\rho_0^2$, so that, for instance, the non-dimensional transverse displacement becomes $\tilde{w} \equiv w\rho_0/m$. In what follows the tildes are dropped, so that from now on all quantities will be non-dimensional unless explicitly stated otherwise. The problem described in the previous paragraph can be solved by using Fourier transforms in x and t, with for instance

$$\bar{w}(k, \omega) = \int_{-\infty}^{\infty}\int_{-\infty}^{\infty} w(x, t)\exp(-\mathrm{i}kx + \mathrm{i}\omega t)\,\mathrm{d}x\,\mathrm{d}t \tag{12}$$

and by transforming equations (2) and (3), completing some algebra, and then inverting the expressions for $\bar{w}$ and $\bar{\theta}$, the solution is found in the form

$$\begin{aligned} w(x,t) &= \frac{1}{4\pi^2}\int_C \exp(-\mathrm{i}\omega t)\int_{-\infty}^{\infty} \frac{\bar{q}_w\,[C\omega^2 - A - Dk^2] - \mathrm{i}kA\bar{q}_\theta}{\mathscr{D}(k,\omega)}\exp(\mathrm{i}kx)\,\mathrm{d}k\,\mathrm{d}\omega, \\ \theta(x,t) &= \frac{1}{4\pi^2}\int_C \exp(-\mathrm{i}\omega t)\int_{-\infty}^{\infty}\left[\frac{\bar{q}_\theta((k^2A^2/\mathscr{D}(k,\omega)) - 1)}{C\omega^2 - A - Dk^2} + \frac{\mathrm{i}kA\bar{q}_w}{\mathscr{D}(k,\omega)}\right]\exp(\mathrm{i}kx)\,\mathrm{d}k\,\mathrm{d}\omega. \end{aligned} \tag{13}$$

Here dimensionless quantities relating to material properties are

$$A = \Gamma m^2/D_1\rho_0^2, \qquad B = I_1\rho_0^2/m^3, \qquad C = I_2\rho_0^2/m^3, \qquad D = D_2/D_1, \tag{14}$$

the non-dimensional flow speed is $U = U_s m^{3/2}/(D_1^{1/2}\rho_0)$; and the dispersion function, $\mathscr{D}(k,\omega)$, is defined by

$$\mathscr{D}(k,\omega) = \left(-k^4 - Ak^2 + \omega^2 + \frac{(\omega - kU)^2}{|k|} + Bk^2\omega^2\right)(Dk^2 + A - C\omega^2) + A^2k^2, \tag{15}$$

where $|k| = \pm k$ for $\mathrm{Re}(k)$ positive and negative respectively. Finally, note that the spatial inversion contour in equation (13) has been chosen to be the real k-axis, while the temporal inversion contour $\mathscr{C}$ is located in the upper half of the ω plane above all the singularities of the integrands of equation (13). Since the point forces are turned on at $t = 0$, it follows that $\bar{q}_{w,\theta}(\omega)$ are analytic in the upper half of the ω plane. In order to fix $\mathscr{C}$ it is therefore necessary to consider just the poles arising from the roots of the full dispersion relation

$$\mathscr{D}(k, \omega) = 0, \tag{16}$$

corresponding to modes in which (to a greater or lesser extent) both shear and flexural motions are excited. In equation (13b) there is apparently another set of poles arising from the roots of

$$C\omega^2 - A - Dk^2 = 0, \tag{17}$$

but closer inspection of equation (13b), together with equation (15), reveals that the residue of the integrand at these points is in fact zero, so that no modes are actually generated. In fact, the dispersion relation (17) corresponds to pure shearing motion in which $w(x, t) = 0$, but from equations (2) and (3) it is clear that this sort of motion could only occur when the coupling between the shearing and flexural motion vanishes (i.e., $\Gamma = 0$). However, it will be seen that certain roots of the full dispersion relation (16) are approximately equal to the roots of equation (17), corresponding to modes in which shear motion dominates.

Once $\mathscr{C}$ has been chosen to lie above all singularities in the ω plane, it follows that for $t < 0$ the temporal contour is closed in the upper half-plane to yield $w = \theta = 0$, thereby guaranteeing that the solution is causal.

2.2. LONG-TIME LIMIT

In principle, the inversion integrals (13) can be computed numerically for arbitrary values of t, but considerable physical insight and simplification can be obtained in the steady state limit $t \to \infty$. The crucial aim here must be to determine the long-time limit of the *causal* solution, and a well-known procedure for doing this has been developed by Briggs [7] and Bers [8], and it was precisely their technique which was applied to fluid–structure interactions by Brazier-Smith and Scott [9], Crighton and Oswell [10], Peake [13] and Lingwood and Peake [14], amongst others.

The idea is to deform the temporal contour $\mathscr{C}$ downwards towards the real ω-axis, while at the same time deforming the spatial inversion contour off the real k-axis so as to avoid any pole crossings and thereby retain an analytical solution. A number of possibilities can occur.

1. Two poles from opposite halves of the k plane could pinch together as $\mathscr{C}$ is lowered, say at $k = k_0$ for $\omega = \omega_0$. Once this happens, downward deformation of $\mathscr{C}$ must be halted, and it can then be shown (see reference [9]) that the long-time behaviour of the system is dominated by the pinching mode, with response proportional to $\exp(-\mathrm{i}\omega_0 t + \mathrm{i}k_0 x)$. Since $\mathrm{Im}(\omega_0) > 0$ (otherwise the pinch would not be found before $\mathscr{C}$ had reached the real ω-axis), it follows that the response grows exponentially in t for all x, which is known as *absolute instability*. Note that necessary and sufficient conditions for absolute instability are the existence of a saddle point (i.e., point where $\partial\omega/\partial k = 0$), which is formed by the coalescence of modes from *opposite* halves of the k plane.

2. If no pinching occurs, then $\mathscr{C}$ can be deformed all the way onto the real axis. It might then be the case that a mode originating in the upper half of the k plane moves below the

k-axis, causing the spatial contour to be deformed downwards. Such a mode would then have a spatial wavenumber with a negative imaginary part, but would be located in $x > 0$ (because it lies above the inversion contour), and therefore corresponds to a *convective instability*.

3. Another possibility is that spatial poles come to rest on the real k-axis once $\mathscr{C}$ has reached the real ω-axis, and therefore correspond to neutral modes. The question of the spatial location of these neutral modes is answered by considering from which half-plane they originated; for instance, a mode which originates from the upper/lower half-plane and moves monotonically onto the real k-axis causes the spatial inversion contour to be indented below/above the pole, and therefore, to a mode located downstream/upstream of the driver. Such modes would have group velocity pointing away from the driver, which conforms with the usual and expected radiation condition of out-going group velocity formulated by Rayleigh [15] and Lighthill [16]. Alternatively, it may happen that a mode originates in the upper half of the k plane, and then moves below the real k-axis as $\mathscr{C}$ is lowered, before returning to the real k-axis once $\mathrm{Im}(\omega)$ has reduced to zero. Such a mode would be located downstream of the driver, but would have its group velocity pointing towards the driver, in violation of the Rayleigh–Lighthill radiation condition.

As already pointed out, the poles in the k plane correspond to the roots of $\mathscr{D}(k, \omega) = 0$, and it will be seen that they exhibit all the types of behaviour enumerated above over significant portions of parameter space.

2.3. MATERIAL PARAMETER VALUES

It is clear that the large number of parameters in this problem leads to some complexity, particularly since the dimensionless quantities A, B, C, D and U are non-linear functions of the thickness, density and transverse and longitudinal Young's modulus ratios ε, δ, γ and g. In order to fix ideas and to indicate the range of parameter values which might be relevant in practice, the sandwich panel described by Nilsson [4] is considered. It is therefore supposed that the skin and core materials are isotropic, with Young's moduli $E_a = 1{\cdot}67 \times 10^{10}$ N/m^2 and $E_b = 0{\cdot}013 \times 10^{10}$ N/m^2, respectively, leading to $\gamma = g = 0{\cdot}0078$; that the material densities are $\rho_a = 1760$ kg/m^3 and $\rho_b = 130$ kg/m^3, leading to $\delta = 0{\cdot}074$; that the Poisson ratio is $\nu = 0{\cdot}3$ in both materials; and finally that the core thickness is 50 mm. The precise materials considered by Nilsson are not given in reference [4], but a typical sandwich panel might be composed of a soft PVC core and stiff carbon fibre/epoxy skin. However, the skin thickness, and hence ε, will be allowed to vary (Nilsson has $\varepsilon = 0{\cdot}1$), and this should thereby provide a consistent picture of the way the dimensionless quantities vary for given skin and core materials. In Figure 2, A,B,C,D/100 are plotted against ε, and all these quantities seem to take $O(1)$ values, which vary quite substantially, as ε increases from zero. As well as these material properties, the fluid density must be specified, which is taken to be that of water, so that $\rho_0 = 1000$ kg/m^3. The dimensionless flow-speed parameter U is simply proportional to the flow speed U_s, but has non-linear dependence on ε through the plate mass m. In Figure 3, U is plotted against ε for a dimensional flow speed $U_s = 10$ m/s and with $\gamma = 0{\cdot}0078$ as above, and again it is seen that U varies significantly as ε is increased. Also plotted is the behaviour of U with the smaller value of $\gamma = 0{\cdot}00078$, corresponding to an even less rigid core material, in order to demonstrate that the value of U is very sensitive to the material properties. It is noted, however, that U is always small here (indeed to obtain $O(1)$ values of U one will typically require unrealistically large flow speeds), and this will allow asymptotic analysis to be completed in the limit of small U in due course. Finally, in this section, it is worth emphasizing the physical interpretation of the

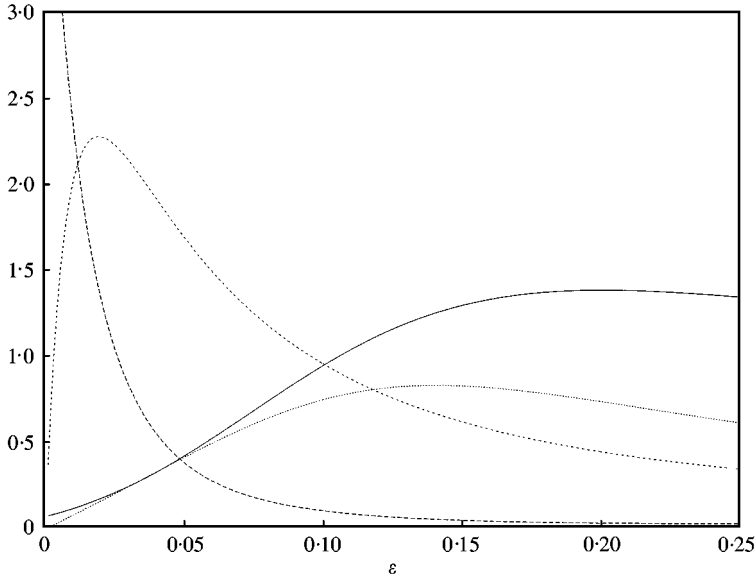

Figure 2. Variation of dimensionless material parameters A, B, C and D, as the thickness ratio ε is varied: ——, A; – – – –, B; -------, C; ....., $D/100$.

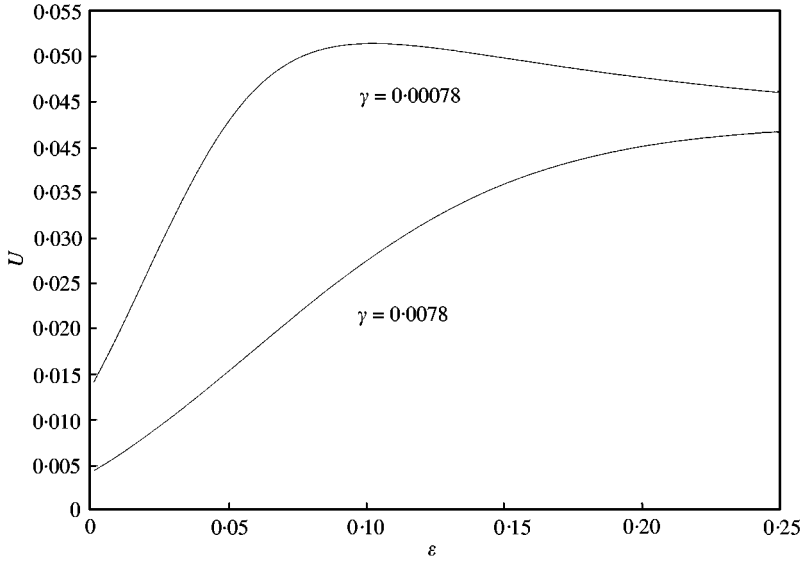

Figure 3. Variation of dimensionless speed parameter U as the thickness ratio ε is varied, with $\gamma = 0{\cdot}0074$, as in reference [4] and also $\gamma = 0{\cdot}00074$.

material parameters. It will be seen that the most significant parameter will be D, the ratio of the effective stiffnesses to longitudinal and transverse motions, and this is large over the parameter range thanks to the relatively small value of ε and γ. The parameter A will also be seen to be significant, and this corresponds (through its proportionality to Γ) to the strength of coupling between the transverse and longitudinal motion. The terms B and C will prove to be less significant in subsequent analysis, but correspond to the rotational terms in the

two equations of motion (note that B approaches a finite value, about 4·93 in this case, as $\varepsilon \to 0$).

3. ABSOLUTE INSTABILITY

In this section, the occurrence of absolute instability for the dispersion relation (16) is described. It turns out that two k modes originating from opposite half-planes can coalescence as ω is reduced, corresponding to absolute instability, provided that the coalescence occurs when $\mathrm{Im}(\omega) > 0$. In order to find the boundary of parameter space over which this can occur, the asymptotic limit of small U is considered first, as was done by Crighton and Oswell [10]. In reference [10] it was shown that in the simple plate problem, absolute instability can occur when $k = O(U^{2/3})$ and $\omega = O(U^{5/3})$, and upon adopting these scalings it is found that there is a preferred limit $A = O(U^{4/3})$ and $D = O(U^{-2/3})$, in which case the full dispersion relation (16) reduces to

$$-k^4 + \omega^2 + \frac{(\omega - kU)^2}{|k|} - Ak^2 + \frac{A^2}{D} = 0, \tag{18}$$

where terms of size up to $O(U^{10/3})$ have been retained. Note that this asymptotic dispersion relation depends only on A, D and U, and the remaining parameters B and C appear only at higher order. By following [10], the absolute instability boundary for this new dispersion relation can now be determined. The absolute instability occurs when two roots coalesce, and the boundary of absolute instability is when a third mode also coalesces with these two modes, leading to a triple root of equation (18) in the k plane. Double differentiation of equation (18) leads to the cubic

$$k^3 + \frac{3A}{10}\,k - \frac{U^2}{10} = 0 \tag{19}$$

and it is easy to show that this equation always has a single real, positive root, which can easily be determined numerically for a given value of A. The corresponding value of ω can then be found from equation (18), and an implicit relationship between U, A and D found by substituting these values for k and ω into the first derivative of equation (18). This therefore yields an asymptotic absolute instability boundary, which for instance can be plotted in A–U space for different values of D, and this is done in Figure 4. Here, the flow is absolutely unstable above each curve. For $A = 0$, corresponding to the case in which the core material has zero stiffness, all the curves go through the point $U \approx 0{\cdot}074$ (the absolute instability boundary found in reference [10]), but as A is increased the value of the flow speed required for absolute instability rises quite rapidly. The boundary is relatively insensitive to D, but tends to move to higher values of U as D is increased.

The absolute instability boundary for the full dispersion relation (16) can be calculated numerically, with the results described above providing a useful first guess. This involves determining the location of a given unstable pinch, and then, for instance, keeping U, B, C and D fixed while A is increased until the saddle frequency becomes real. This can then be repeated for other values of U to build up the absolute instability boundary in the A–U plane, and then repeated for different B, C and D if required. In Figure 5, the absolute instability boundary is plotted as A is varied, with B, C, D taking the values given in reference [4]. Changing the values of B and C has very little effect on this curve, while changing D has the same effect as seen in Figure 4. The boundary has been continued up to $U = 1$, which for the panel described in reference [4] corresponds to the unrealistically large dimensional flow speed of 365·5 m/s! Interestingly, for U larger than about 1, it no longer

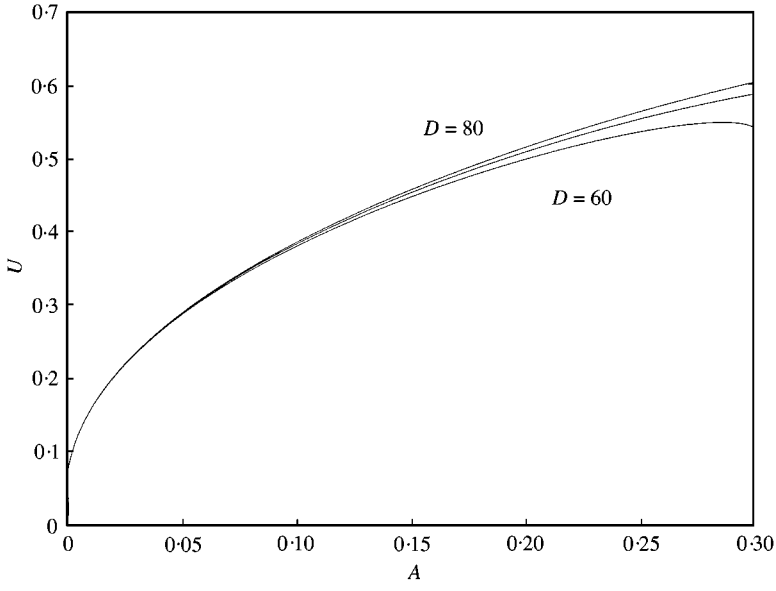

Figure 4. Absolute instability boundary for small U in the A–U plane, for $D = 60$, 70, 80, from equation (18). The flow is absolutely unstable above and to the left of each curve.

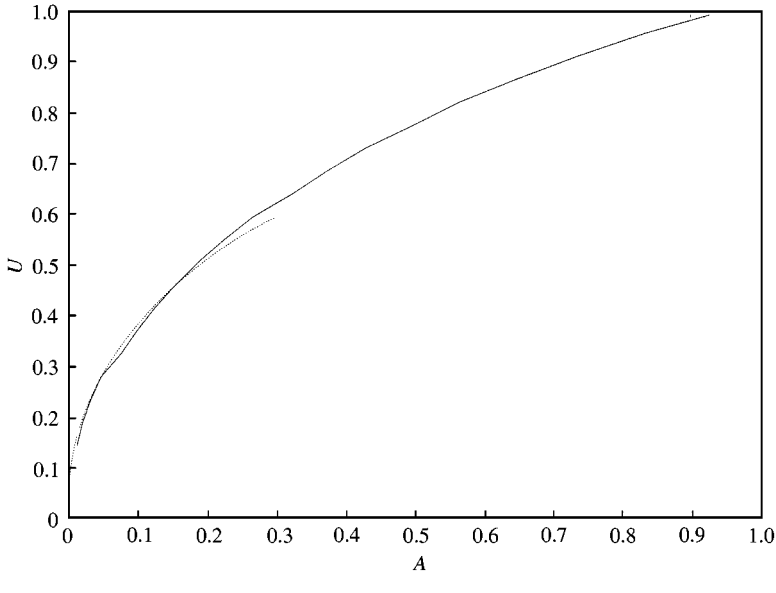

Figure 5. Absolute instability boundary (———) for $\varepsilon = 0{\cdot}1$ in the A–U plane, from the full dispersion relation (16). Other material parameters as in reference [4], leading to $B = 0{\cdot}094$, $C = 0{\cdot}951$, $D = 74{\cdot}2$. The small U result (·····) has also been included for comparison.

proved possible to find a value of A for which the unstable saddle becomes neutral, suggesting that the flow might then be absolutely unstable for all A. However, since $U = 1$ appears to be a flow speed which could never be attained in practice, this possibility need not be considered further. Indeed, it seems from the results presented here that absolute instability would be unlikely to occur in practice for typical sandwich panels.

4. CONVECTIVE INSTABILITY AND NEUTRAL MODES

If the flow is not absolutely unstable, then the temporal inversion contour in equation (13) can be deformed down onto the real ω-axis, and this means that conventional spatial or temporal stability analysis can be performed. In Figure 6, the temporal roots of equation (16) for real k are plotted, with material parameter values as in reference [4] and with speed $U = 0{\cdot}025$ (corresponding to a dimensional flow speed of 9·14 m/s). Only the modes with $k > 0$ are considered, and results for $k < 0$ follow by reflecting Figure 6 in the origin. Four solution branches are evident. Two of the branches seen in Figure 6(a) have $\omega = O(1)$, and originate from $\omega = \pm\sqrt{A/C}$ at $k = 0$. These modes are all neutral, and it turns out are approximately, *but not exactly*, equal to the roots of equation (17), which themselves are modes associated with pure shearing of the plate. For this reason, these solution branches will be referred to as the *longitudinal* branches. The second pair of branches are found at much smaller values of ω, and possess the more complicated structure shown magnified in Figure 6(b) and 6(c). For $k < k_b$ there is a pair of complex modes, one of which corresponds to a convective instability, at $k = k_b$ the branches coalesce, and for $k > k_b$ there is a pair of neutral modes. This structure is in fact very similar to that found in reference [10] for a conventional plate, so that these modes can be associated with the transverse motion of the panel (i.e., $w \neq 0$), and will be referred to as the *transverse* branches. In this case, the coupling between the shear and flexural motions will be seen to be significant.

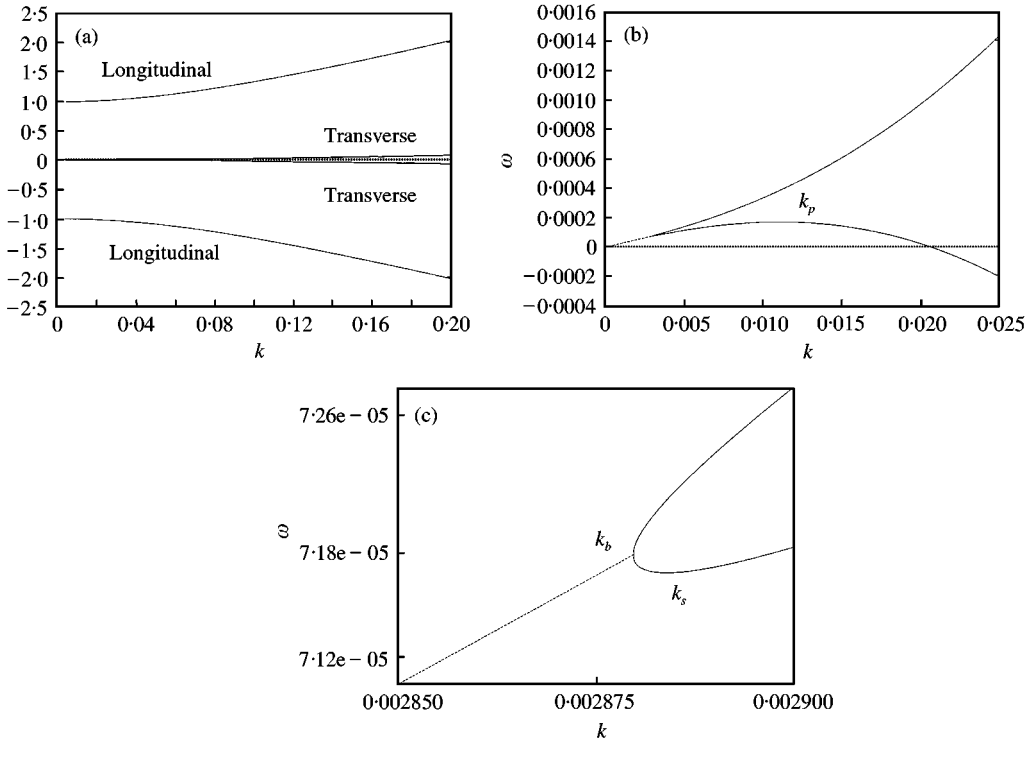

Figure 6. Roots of the dispersion relation (16) for real k ((b) and (c) are successively magnified views of (a)), with material parameter values $A = 0{\cdot}938$, $B = 0{\cdot}094$, $C = 0{\cdot}951$, $D = 74{\cdot}200$ and $\varepsilon = 0{\cdot}1$, and with flow speed parameter $U = 0{\cdot}025$. The solid lines correspond to neutral modes, and the dotted line in (b) and (c) to the real part of a convectively unstable mode.

4.1. ANALYSIS FOR SMALL U

In order to understand the model structure of the present problem, it is helpful to apply first asymptotic analysis in the limit of small U (note from Figure 3 that this is an entirely realistic limit). The aim is to describe all of the k–ω plane over which mean-flow effects are important, and following Crighton and Oswell [10] $k = O(U)$ is considered first. The transverse branches will have $\omega = O(1)$, and writing $k = UK$, $\omega = \Omega + U\Omega_1 + \ldots$, with quantities denoted by a capital letter being $O(1)$, and then substituting this into the full dispersion relation (16) and equating powers of U, it is found that

$$\omega = \pm \left\{ \frac{A^{1/2}}{C^{1/2}} + \frac{U^2 D K^2}{2A^{1/2}C^{1/2}} + \frac{U^3 K^3 A^{1/2} C^{1/2}}{2} + O(U^4) \right\}. \tag{20}$$

The first two terms in this expansion are identical to the equivalent expansion of ω for purely transverse motion from equation (17), and it can therefore be seen that for these modes the coupling of the flexural motion to the shear motion is very weak, and has an effect of size only $O(U^3)$ on the modal frequency. In the same way, the longitudinal branches can be determined for $k = O(U)$ by writing $\omega = U^2\Omega_0 + U^{5/2}\Omega_1 + U^3\Omega_2 + \ldots$, and again substituting this into equation (16) and equating powers of U the two branches

$$\begin{aligned} \omega = {} & U^2 K \pm U^{5/2} \left[K^5(D+1) - K^3\right]^{1/2} \\ & - U^3 K^2 \pm \frac{U^{7/2}\left[2K^4 - K^6(D+1)\right]}{2\left[K^5(D+1) - K^3\right]^{1/2}} + O(U^4) \end{aligned} \tag{21}$$

are found. Note that only the material parameter D features in these terms, indicating that it is the relative stiffnesses of the skin and core which is crucial at this order. Moreover, if $D = 0$, corresponding to zero core stiffness, then this expansion matches exactly with that obtained for a simple thin plate in reference [10]. The branch point k_b can be obtained by noting, via the Binomial Theorem, that the sum of the terms with alternating signs in equation (21) is equal to

$$\left[K^5(D+1) - K^3 + U\left(2K^4 - K^6(D+1)\right)\right]^{1/2} \tag{22}$$

to the asymptotic order considered, and setting this quantity equal to zero yields

$$\begin{aligned} k_b &= \frac{U}{\sqrt{D+1}} - \frac{U^2}{2(D+1)} + O(U^3), \\ \omega_b &= \frac{U^2}{\sqrt{D+1}} - \frac{3U^3}{2(D+1)} + O(U^4). \end{aligned} \tag{23}$$

For the parameter values used in Figure 6, this gives the asymptotic estimates $k_b = 0{\cdot}0028788$ $\omega_b = 7{\cdot}176 \times 10^{-5}$, which compares very well with the exact values of $0{\cdot}0028797$ and $7{\cdot}180 \times 10^{-5}$ respectively. The branch point corresponds to an exceedingly low-frequency, long-wave mode; for the parameter values given in reference [4], the corresponding wavelength is 52·6 m and the frequency is 0·17 Hz. In contrast to this, the longitudinal branch arises at a much higher frequency; for instance, $\omega = \sqrt{A/C}$ is equivalent to a frequency of about 2·4 kHz. Of course, the present theory will break down for wavelengths which are comparable to, or shorter than, the thickness of the whole panel. The sandwich thickness has been taken to be 0·06 m, so that a mode with wavelength

shorter than this thickness would have dimensionless wavenumber larger than about 2·25. It therefore follows that all the modes shown in Figure 6 have wavelengths which are significantly longer than the transverse dimensions of the plies. Of course, it might alternatively be argued that a frequency of 2·4 kHz leads to a short acoustic wave. In the current paper, incompressible flow has been assumed, so that the acoustic wavelength is infinite and the theory is self-consistent. However, taking instead a sound speed of 1500 m/s in water, this frequency leads to an acoustic wavelength of 0·625 m, which is again considerably thicker than the panel.

The zero group velocity point $k = k_s$ on the lower transverse branch is also described by the scaling $\omega = O(U^2)$. The leading-order expression for k_s could be determined by differentiating equation (21) with respect to K, but in order to distinguish k_s from the branch point k_b a higher order approximation is required, and to obtain this it proves easier to first determine k as a function of ω, thereby effectively inverting expansion (21). After some algebra this turns out to be

$$k = U\Omega \pm U^{3/2}\left[(D+1)\,\Omega^5 - \Omega^3\right]^{1/2} + U^2\,\frac{5(D+1)\Omega^4 - \Omega^2}{2}$$

$$\pm U^{5/2}\,\tfrac{5}{2}\,\Omega^3(1+D)\left[(D+1)\,\Omega^5 - \Omega^3\right]^{1/2} \tag{24}$$

$$\pm U^{5/2}\,\frac{\left[5(D+1)\Omega^4 - \Omega^2\right]^2}{8\left[(D+1)\,\Omega^5 - \Omega^3\right]^{1/2}} + O(U^3)$$

and the second and fifth terms taken together yield the turning point in the form

$$k_s = \frac{U}{\sqrt{D+1}} + O(U^{5/2}), \qquad \omega_s = \frac{U^2}{\sqrt{D+1}} - \frac{2U^3}{D+1} + O(U^{7/2}). \tag{25}$$

For the parameter values used in Figure 6, this gives the asymptotic estimate for the point (k_s, ω_s) as $(0{\cdot}002877,\ 7{\cdot}1657 \times 10^{-5})$, which again compares very well with the exact values of $(0{\cdot}00288395,\ 7{\cdot}1680 \times 10^{-5})$. With $D = 0$ equation (25) again agrees exactly with the corresponding result from reference [10].

The turning point $k = k_p$ in Figure 6(b) is not described by the scaling used in the previous paragraph, and to describe this the alternative scaling $k = U^{2/3}K$ is used by following reference [10]. Proceeding in exactly the same way, the longitudinal modal frequencies are given by

$$\omega = \pm\left\{\left(\frac{A}{C}\right)^{1/2} + \frac{U^{2/3}}{2}\left(\frac{A}{C}\right)^{1/2} + O(U^{4/3})\right\} \tag{26}$$

and are therefore independent of wavenumber to this asymptotic order (explaining why the corresponding curves in Figure 6 are relatively flat for k less than about 0·01). Interestingly, only the first term in equation (26) now agrees with the corresponding expansion for the completely uncoupled transverse modes from equation (17), so that the effect of the coupling to the flexural motion now arises earlier, at $O(U^{2/3})$, than when $k = O(U)$. The modal frequencies on the transverse branches are now given by

$$\omega = U^{5/3}(K \pm K^{5/2}\,(1+D)^{1/2}) - U^{7/3}K^2 \mp U^{7/3}\,\frac{K^{7/2}\,(1+D)^{1/2}}{2} + O(U^3). \tag{27}$$

By differentiating this result with respect to K and considering the negative root, the leading-order terms in the expansion for the turning point k_p on the transverse branch are found in the form

$$k_p = U^{2/3}\left(\frac{4}{25(1+D)}\right)^{1/3} + O(U^{4/3}),$$
$$\omega_p = \frac{3U^{5/3}}{5}\left(\frac{4}{25(1+D)}\right)^{1/3} + O(U^{7/3}). \tag{28}$$

Again, the agreement between the asymptotic turning point ($0{\cdot}010997$, $1{\cdot}6495 \times 10^{-4}$) and the exact result ($0{\cdot}011002$, $1{\cdot}6687 \times 10^{-4}$) is very satisfactory—higher order terms could be calculated, as in the previous paragraphs, but will not be needed in subsequent analysis and can therefore be omitted. In dimensional terms, again using parameters from reference [4], this point corresponds to a wavelength of $13{\cdot}8$ m and a frequency of $0{\cdot}4$ Hz.

The dispersion curves for small k has now been completely described. For $k = O(1)$, it is easy to see that mean-flow effects do not enter the solution to leading order, and that one is simply left with the zero-flow problem described in reference [6].

4.2. SPATIAL LOCATION OF MODES

The only unstable modes present in Figure 6 are located on the transverse branches for $\omega < \omega_s$. In fact, there is a pair of complex conjugate roots here, which have originated in the upper half of the k plane for large $\mathrm{Im}(\omega)$, and as described in section 2.2, point 2, the spatial inversion contour is deformed below the mode in the lower half-plane, which therefore corresponds to a convectively growing mode downstream of the driver. The conjugate mode corresponds to an evanescent wave downstream. The system is therefore convectively unstable when driven at $\omega < \omega_s$; note that the temporal growth rate approaches zero as ω approaches zero.

All the other modes shown in Figure 6 are neutral. The transverse mode with $k_b < k < k_s$, $\omega_s < \omega < \omega_b$ possesses exactly the property described in section 2, point 3, whereby it originates in the upper half of the k plane for large $\mathrm{Im}(\omega)$, moves below the real k-axis as $\mathrm{Im}(\omega)$ is reduced, and then turns round and moves onto the real axis as $\mathrm{Im}(\omega) \to 0$—see Figure 7. This means that the mode is located downstream of the driver, because it originated in the upper half of the k plane, but possesses a group velocity directed towards the driver, because it moves onto the real k-axis from below. This violates the usual radiation condition of out-going group velocity at infinity, as formulated by Rayleigh [15] and Lighthill [16], and is exactly the behaviour found by Crighton and Oswell [10] in their simple-plate problem. Of course, the Rayleigh–Lighthill radiation condition was developed for situations in which the driver is the only source of energy, whereas in the present problem energy can be extracted from the mean flow as well—this is described fully in reference [10]. However, this "anomalous" behaviour demonstrates that in general the causal solution to initial value problems must be determined using the sort of global consideration of the dispersion function described here, and not merely via local behaviour based on the group velocity. All the other neutral modes in Figure 6, including the rest of the transverse branches and both longitudinal branches, behave in a conventional way, with group velocity directed away from the driver. From equation (23) and (25) it can be seen that the anomalous frequency range has length $U^3/2(D+1)$, which is of course very

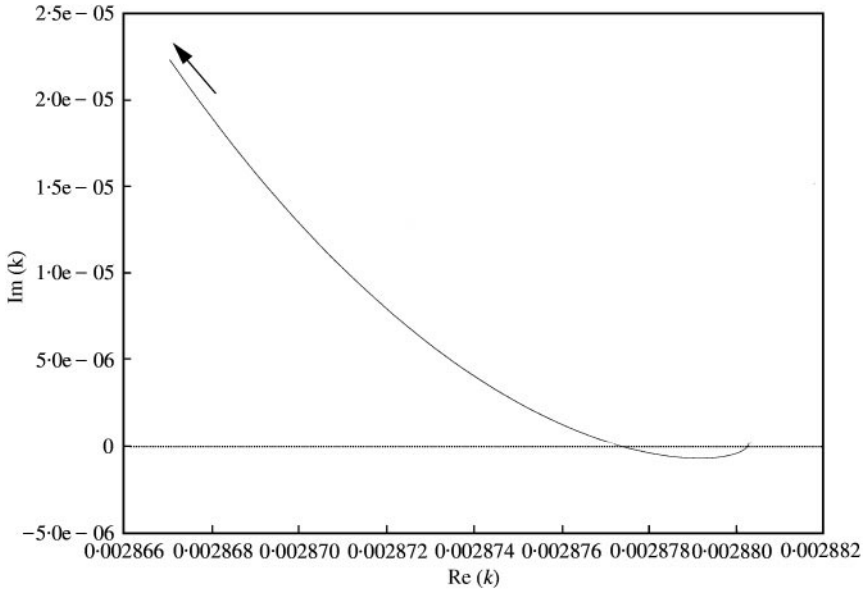

Figure 7. Movement (in direction of arrow) of the mode $k = 0{\cdot}0028803$, $\omega = 7{\cdot}17234 \times 10^{-5}$ as $\mathrm{Im}(\omega)$ is increased from zero. Parameter values as in Figure 6.

small, and therefore over most frequencies the Rayleigh–Lighthill criterion is entirely applicable. Since D is moderately large in the present calculations, the anomalous frequency range found here is even smaller in length than that found by Crighton and Oswell [10], who had $D = 0$.

4.3. AMPLITUDE OF RESPONSE

The asymptotic results derived in this section will now be used to investigate the amplitude of neutral waves excited by the driver. If it is supposed that the driver acts with a single frequency, ω, and the flow is not absolutely unstable, then the plate deflection far from the driver can be obtained simply from equation (13) as a sum of contributions from the corresponding k poles at the given ω. It is also clear that in general the amplitude of a given mode will contain a component which is proportional to the force q_w and a component which is proportional to the couple q_θ, and the aim here is to ascertain the relative amplitudes of these two terms.

First, consider neutral modes corresponding to the transverse branches of the full dispersion relation (16), and for definiteness consider the preferred limit $\omega = O(U^2)$. In this range, the dispersion relation (16) has two roots with $k = O(U)$, described by equation (21), and it is easy to show that for both these roots the corresponding plane-wave surface deflections are

$$w(x, t) = O(U^{-1})\,\bar{q}_w + O(1)\bar{q}_\theta,$$
$$\theta(x, t) = O(1)\bar{q}_w + O(U)\bar{q}_\theta\,, \tag{29}$$

from which it can be concluded that the deflections are here more strongly coupled to the force than to the moment, and indeed that the flexural deflection is larger than the shear

deflection. Also, equation (16) has two other roots with $k = O(U^{2/3})$, for which it is easy to show that equation (29) also applies, but with U replaced by $U^{2/3}$. Exactly equivalent analysis in the second preferred limit $\omega = O(U^{5/3})$ will lead to the same conclusion, and it can therefore be said that for modes on the transverse branches the response is dominated by the force, and that the flexural motion is significantly larger than the shear motion.

Second, consider neutral modes on the longitudinal branches of the full dispersion relation (16). For $\omega = \sqrt{A/C} + O(U^2)$, as described by equation (20), there is a neutral mode with $k = O(U)$, for which it can be shown that

$$w(x, t) = O(U^2)\,\bar{q}_w + O(1)\bar{q}_\theta,$$
$$\theta(x, t) = O(1)\bar{q}_w + O(U^{-2})\bar{q}_\theta. \tag{30}$$

Hence, in this regime it is the point *moment* which is much more strongly coupled to the plate deflections, and the shear deflection is much larger than the flexural deflection. Interestingly, however, if ω is a little further away from $\sqrt{A/C}$, say by $O(U^{2/3})$ as described by equation (26), then the four coefficients in equation (30) are all $O(1)$, and the force and moment now make contributions of equal order. It can therefore be concluded that the plate must be driven with a frequency very close to $\sqrt{A/C}$ in order for shear motion to dominate the response. Similar results are obtained in the companion paper [6] in the absence of mean flow.

5. ENERGY

In this section, the energy balance in the system will be considered, with particular reference to how the various modes described in the previous section contribute to the energy flow out of, and indeed into, the driver. It will still be supposed that the system is below the absolute instability boundary described in section 3, so that if the driver oscillates with a single real frequency ω then the system will respond with the same frequency, with the long-time limit of the causal response being given via the Briggs–Bers technique described earlier.

5.1. WAVE ENERGY

The wave energy of a neutral mode in the system will be calculated first. This concept was introduced by Benjamin [17] and Landahl [18], and formulated in the context of fluid loading by Cairns [19], and corresponds to the work done to create the neutral wave at $t = O(1)$ starting from rest at $t = -\infty$. Consider a wave with flexural deflection $w = A(t)\exp(\mathrm{i}kx - \mathrm{i}\omega t)$, and corresponding shear deflection, where k is a root of equation (16) for the given ω, and $A(t)$ is the wave amplitude which increases only slowly with t. Work must be done to create the wave, and this corresponds to the working of the tranverse surface velocity against the difference between the hydrodynamic pressure exerted by the fluid on the panel and the equivalent pressure exerted by the panel on the fluid (these two pressures are in balance only when the wave has become a normal mode.) From the left-handside of equation (2) and from equation (10), it is easy to see that this pressure difference is

$$\mathscr{D}_w(k, \omega + \mathrm{i}\,\partial/\partial t)\,A(t)\exp(\mathrm{i}kx - \mathrm{i}\omega t), \tag{31}$$

where the time derivative is supposed to act only on $A(t)$, and where the new dispersion function is

$$\mathscr{D}_w(k, \omega) \equiv \mathscr{D}(k, \omega)/(Dk^2 + A - C\omega^2). \tag{32}$$

By following Cairns, it can be shown that the work done to create the wave (the wave energy) is

$$\frac{1}{4}\left(\omega \frac{\partial \mathscr{D}_w}{\partial \omega}\right)|A|^2 \tag{33}$$

and for convenience the wave energy per unit amplitude, E, is introduced, which is simply obtained from equation (33) by setting $A = 1$.

For solutions of equation (16) it follows from equation (33) that the wave can be either a positive energy wave ($E > 0$) or a negative energy wave ($E < 0$), depending on the sign of $\omega(\partial D_w/\partial\omega)$. The excitation of positive energy waves leads to an increase in the total system energy, while excitation of negative energy waves lead to a decrease in total system energy. It is a straightforward matter to check numerically, and to verify asymptotically for small U, that in Figure 6 the modes on the longitudinal branches are all positive energy waves, while the modes on the lower transverse branch between $k = k_b$ and the point where the branch crosses $\omega = 0$ are negative energy waves (the modes on the remaining portions of the transverse branches are positive energy waves). The behaviour of the wave energy for the transverse branches is exactly the same as found by Crighton and Oswell [10].

Having associated a wave energy with a given neutral mode, an energy flux per unit amplitude in the direction *away* from the driver can be defined as

$$J(k, \omega) = \pm \frac{\partial \omega}{\partial k} E, \tag{34}$$

where the group velocity $\partial\omega/\partial k$ is the velocity of energy propagation, and the plus and minus signs correspond to modes downstream and upstream of the driver respectively. The sign of J will determine whether a mode transports energy away from the driver ($J > 0$) or towards the driver ($J < 0$). From the remarks made in the previous paragraph, it is clear that the pure shear modes all have $J > 0$, as do the modes on the upper transverse branch. The modes with $\omega > 0$ on the lower transverse branch are all negative energy waves ($E < 0$); for $k > k_s$ they also have group velocity directed away from the driver, and therefore have $J < 0$; but for $k_b < k < k_s$ the anomalous mode has group velocity directed towards the driver, yielding $J > 0$. In the next section it will be seen how all these modes balance to give a total net energy flux which can be either positive or negative, depending on the value of ω.

5.2. WORK DONE BY DRIVER

The total rate of working by the driver is made up of the work done by the force q_w and the couple q_θ, and for a single oscillation frequency, ω, the time-average rate of working, $\mathscr{W}$, is equal to

$$\mathscr{W} = \tfrac{1}{2}\,\mathrm{Re}\{-\mathrm{i}\omega w q_w^* - \mathrm{i}\omega\theta q_\theta^*\}. \tag{35}$$

Expressions for w and θ for real ω can easily be found from equation (13) by suppressing the ω integration and suitably deforming the spatial contour around any poles according to the Briggs–Bers procedure. In fact, the spatial integrals possess both real and imaginary parts, but it is only the imaginary parts, which come from the contributions arising from deformation above or below neutral, or below convectively unstable, poles which contribute

to the rate of working. The real parts of the k integrals, which are just Cauchy principal-value integrals, only affect the near field of the driver. Hence, by substituting results from equation (13) into equation (35), and after some algebra, the rate of working becomes

$$\mathscr{W} = \frac{\omega^2}{16} \sum \frac{1}{J(k(\omega), \omega)} \left| q_w - \frac{\mathrm{i}kAq_\theta}{Dk^2 + A - C\omega^2} \right|^2 . \tag{36}$$

The terms in equation (36) arise from the poles corresponding to the roots of equation (16), and for $\omega > \omega_s$ the summation runs over all the real k roots of equation (16) for the given real ω. For $\omega < \omega_s$, the flow is convectively unstable, and the summation then also involves the corresponding unstable mode, the contribution from which must be interpreted as just the real part of $1/J$. In equation (36) the residue contributions from the poles have been rewritten in terms of the energy flux $J(k(\omega), \omega)$ by using the results

$$(Dk^2 + A - C\omega^2) \frac{\partial \mathscr{D}_w}{\partial \omega} = \frac{\partial \mathscr{D}}{\partial \omega} = -\frac{\partial \mathscr{D}}{\partial k} \Big/ \frac{\partial \omega}{\partial k}. \tag{37}$$

Here, the first result follows from taking the ω derivative of equation (32), and the second result comes from the chain rule applied to the ω derivative of equation (16).

The form of equation (36) is very important, and confirms the interpretation of wave energy given at the end of the previous subsection. The sign of the contribution from a given mode depends only on the sign of the energy flux $J(k(\omega), \omega)$ of that mode, since clearly the amplitude of the contribution is always positive definite. The rate of working is plotted in Figure 8 in two different cases, one in which the point source produces a force but zero torque, and a second in which the source produces both a force and a torque of equal dimensionless amplitude which are exactly in phase. Just two ranges of ω are plotted—one for small ω and the second for $\omega \approx \sqrt{A/C}$—and outside these ranges the work simply decreases monotonically with increasing ω. For small ω, the rate of working is dominated by the contribution from the force, so that in fact the two curves are indistinguishable in Figure 8(a). Note that rate of working is negative for all $\omega < \omega_p$, indicating that the waves with negative energy flux are dominant. Also, the rate of working is divergent at $\omega = \omega_p$. In contrast, in Figure 8(b) the rate of working is always positive (since as noted above no negative energy waves are present for $\omega > \omega_p$). The rate of working of the point force alone, and of the point moment, for $\omega < \sqrt{A/C}$ are small. However, for $\omega \geqslant \sqrt{A/C}$ the real transverse mode makes a significantly larger contribution, and indeed $\mathscr{W}$ becomes infinite at $\omega = \sqrt{A/C}$, since the transverse mode then has $k = 0$, leading to a singularity in the corresponding second term in equation (36). The enhancement of the contribution from the point moment can easily be seen by noting that in equation (36) $\bar{q}_\theta$ appears multiplied by the factor $-\mathrm{i}kA/(Dk^2 + A - C\omega^2)$, which essentially comes from the ratio between θ and w given in the transformed version of equation (3). When ω is small, it was seen in section 4.1 that the roots k of (16) are small, so that this amplitude ratio is also small. This explains why $\bar{q}_\theta \neq 0$ has no appreciable effect in Figure 8(a). However, when ω is close to $\sqrt{A/C}$, it also follows from section 4.1 that $k/(Dk^2 + A - C\omega^2)$ is large (for instance, when $\omega = \sqrt{(A/C)} + O(U^2)$, this factor is $O(U^{-2})$), and hence at these frequencies the couple makes a large contribution to the rate of working.

5.3. ENERGY BALANCE EQUATION

The question of how energy is transported away from, or towards, the driver (i.e., through the fluid or in the panel) is now considered, and to do this it is necessary to derive an energy

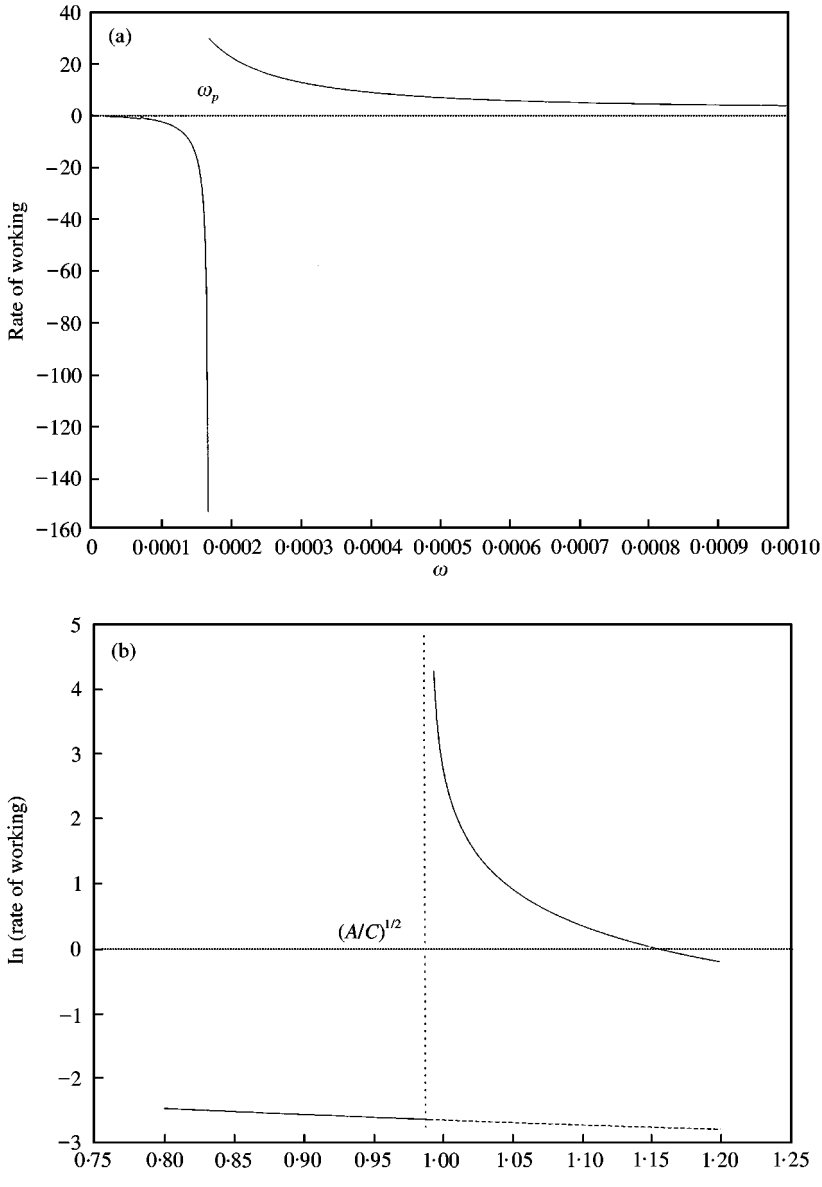

Figure 8. Plots of the rate of working of the source with $q_w = 1$ and $q_\theta = 0$ (.....) and $q_w = 1$ and $q_\theta = 1$ (———), over the two significant ranges of ω. Parameter values as in Figure 6.

balance equation for the system. This proceeds by multiplying equations (2) and (3) by $\partial w/\partial t$ and $\partial\theta/\partial t$, respectively, adding the results together and then integrating in x between $x_1 < 0$ and $x_2 > 0$. The details of this calculation are very similar to those presented in section 4.1 of reference [10], and only the result for the present system need be given here. It turns out that

$$\frac{\mathrm{d}(T_f + T_p + V_p)}{\mathrm{d}t} + F(x_2, t) - F(x_1, t) = q_w \frac{\partial w}{\partial t} + q_\theta \frac{\partial \theta}{\partial t}. \tag{38}$$

The term on the right-hand side is of course the rate of working of the driver, as stated in the previous subsection. On the left-hand side, T_f is the quadratic approximation to the

disturbance kinetic energy in the fluid (exactly as in reference [10], see their equation (4.4)), while T_p and V_p are the kinetic and potential energies of the panel, which in the present problem are different to those of reference [10] and become

$$T_p = \frac{1}{2}\int_{x_1}^{x_2} \left(\frac{\partial w}{\partial t}\right)^2 + C\left(\frac{\partial \theta}{\partial t}\right)^2 + B\left(\frac{\partial^2 w}{\partial x\,\partial t}\right)^2 \mathrm{d}x,$$

$$V_p = \frac{1}{2}\int_{x_1}^{x_2} \left(\frac{\partial^2 w}{\partial x^2}\right)^2 + D\left(\frac{\partial \theta}{\partial x}\right)^2 + A\left(\theta + \frac{\partial w}{\partial x}\right)^2 \mathrm{d}x. \tag{39}$$

In equation (38) the flux term, $F(x, t)$, is given by

$$F = J_f + J_p + J_{pf} \tag{40}$$

with the three terms on the right being the energy fluxes in the fluid and in the plate, and a coupled term respectively. These quantities are

$$\mathrm{J}_f = \int_0^\infty \frac{\partial \phi}{\partial x}\left(p + U\frac{\partial \phi}{\partial x}\right)\mathrm{d}y,$$

$$J_p = \frac{\partial w}{\partial t}\frac{\partial^3 w}{\partial x^3} - \frac{\partial^2 w}{\partial t\,\partial x}\frac{\partial^2 w}{\partial x^2} - B\frac{\partial w}{\partial t}\frac{\partial^3 w}{\partial x\,\partial t^2} - D\frac{\partial \theta}{\partial t}\frac{\partial \theta}{\partial x} - A\left(\theta + \frac{\partial w}{\partial x}\right)\frac{\partial w}{\partial t},$$

$$J_{pf} = Uw\frac{\partial \phi}{\partial t}. \tag{41}$$

Consider now a single mode satisfying equation (16). The time averages (denoted by angle brackets) of the three components of the energy flux become

$$\langle J_p\rangle = \frac{|w|^2}{2}\left\{2\omega k^3 + Ak\omega - Bk\omega^3 + \frac{A^2\omega k(C\omega^2 - A)}{(Dk^2 + A - C\omega^2)^2}\right\},$$

$$\langle J_f\rangle = \frac{|\omega|^2}{4k^2}\omega(\omega - kU)^2, \qquad \langle J_{pf}\rangle = \frac{|w|^2 U}{2k}\omega(\omega - kU)^2. \tag{42}$$

For modes on the longitudinal branch with ω close to $\sqrt{A/C}$, it is easy to show that the plate flux J_p is dominated by the contribution from the transverse deflection θ: i.e., by the final term in the expression for $\langle J_p\rangle$. However, it also turns out that $\langle J_f\rangle$ is the largest of the three fluxes; for instance, for $\omega = \sqrt{A/C} + O(U^2)$ it follows that $k = O(U)$ and hence that $\langle J_f\rangle = O(U^{-2})$, while $\langle J_p\rangle = O(U^{-1})$ and $\langle J_{pf}\rangle = O(1)$. This is perhaps a rather surprising conclusion, because one might expect that for these predominantly shearing modes most of the energy would be carried in the plate. However, it can be understood by noting that the relatively large values of the fluid flux has arisen from the fact that the fluid velocity potential and pressure are proportional to $(\omega - kU)/k$, and on the longitudinal branch there are long wavelength, but relatively high frequency, disturbances, causing this factor to become large. In other words, these in-plane motions induce a piston-like transverse motion of the plate, and because the fluid is assumed incompressible this leads to the build-up of a large unsteady pressure, and hence to a large energy flux through the fluid.

Alternatively, for modes on the transverse branch of equation (16) with ω small, it can be shown that most of the energy is carried in the plate (e.g., for $\omega = O(U^2)$, $k = O(U)$ it turns out that $\langle J_p \rangle = O(U^3)$, while $\langle J_f \rangle = O(U^5)$ and $\langle J_{pf} \rangle = O(U^{9/2})$). In this case, the energy flux in the plate is dominated by the flexural term A $((\partial w/\partial x)$ $(\partial \omega/\partial t))$, and as might be expected the shear motion makes a smaller contribution.

6. CONCLUDING REMARKS

In this paper, the causal response of a sandwich panel to point excitation in the presence of uniform mean flow has been analyzed, and it has been seen how the mean flow leads to a number of unusual features. Crighton and Oswell [10] showed how a simple homogeneous plate in mean flow can exhibit absolute instability, anomalous propagation waves with group velocity directed towards the driver and negative energy waves. All three of these features turn out to be present for the sandwich panel as well. It seems that it is highly unlikely that absolute instability will occur for a typical sandwich panel, since for the realistic panel parameters studied here it is found that the mean flow speed needs to be in excess of exceedingly high values. Indeed, the threshold mean-flow speeds for absolute instability in typical panels are an order of magnitude greater than the value for steel in water found by Crighton and Oswell [10]. The anomalous propagation can occur for realistic panel parameters, but only over a very restricted frequency range. In contrast, it has been seen that negative energy waves can certainly exist over a very wide parameter range, and this is a significant point, since the direction of energy transfer can no longer be assumed to be from the driver to the structure. Indeed, it is known that negative energy waves can play an important role in divergence instability and the onset of flutter in homogeneous plates, and it is reasonable to expect that this could potentially happen for sandwich panels as well.

Energy is transported along the sandwich structure through both the fluid and through the panel (as happens for a homogeneous plate). The latter is made up of contributions from both the transverse motion (again as for a homogeneous plate) and the longitudinal motion associated with shear between the core and skin (which is of course not present for a homogeneous plate). As might be expected, the transverse and longitudinal contributions dominate the plate energy flux for the transverse and longitudinal modes respectively. Interestingly, however, it has been shown that a significant amount of energy can also be transported through the fluid when the panel undergoes shear-dominated deflections, due to the induced long-wavelength but relatively high-frequency transverse motion. This feature is also absent for a homogeneous plate, and may have implications for noise radiation from sandwich panels in flow.

ACKNOWLEDGMENT

The authors gratefully acknowledge financial support provided by the U.S. Office of Naval Research under grant N00014-96-1-1085.

REFERENCES

1. J. N. REDDY 1997 *Mechanics of Laminate Composite Plates*. Boca Raton, FL: CRC Press.
2. A. NOSIER, R. K. KAPANIA and J. N. REDDY 1993 *American Institute of Aeronautics and Astronautics Journal* **31**, 2335–2346. Free vibrations analysis of laminated plates using a layerwise theory.

3. Y. FROSTIG and M. BARUCH 1990 *American Institute of Aeronautics and Astronautics Journal* **28**, 523–531. Bending of sandwich beams with transversally flexible core.
4. A. C. NILSSON 1990 *Journal of Sound and Vibration* **138**, 73–94. Wave propagation in and sound transmission through sandwich plates.
5. M. C. JUNGER and D. FEIT 1986 *Sound, Structures and their Interaction*. Cambridge, Massachusetts: MIT Press.
6. S. V. SOROKIN and N. PEAKE 2000 *Journal of Sound Vibration*. Vibrations of sandwich plates with concentrated masses and spring-like inclusions. (To appear).
7. R. J. BRIGGS 1964 *Electron-stream Interaction with Plasmas*. Cambridge, Massachusetts: MIT Press.
8. A. BERS 1983 in *Handbook of Plasma Physics* (M. N. Rosenbluth and R. Z. Sagdeev, editors), Vol. 1, 451–517. Amsterdam: North-Holland. Space–time evolution of plasma instabilities—absolute and convective.
9. P. R. BRAZIER-SMITH and J. F. SCOTT 1984 *Wave Motion* **6**, 547–560. Stability of fluid flow in the presence of a compliant surface.
10. D. G. CRIGHTON and J. E. OSWELL 1991 *Philosophical Transactions of the Royal Society of London* **335**, 557–592. Fluid loading with mean flow. I. Response of an elastic plate to localised excitation.
11. V. R. SKVORTSOV 1993 *Transactions of Academy of Sciences of U.S.S.R. Mechanics of Rigid Bodies* **1**, 162–168. Symmetrically inhomogeneous through thickness plate as a sandwich plate having a soft core (in Russian).
12. V. R. SKVORTSOV 1998 *Proceedings of Fourth Conference on Sandwich Construction, Stockholm*, Vol. 1, 208–219. KTH Press. Influence of boundary effects of vortex-type on bending of sandwich plates.
13. N. PEAKE 1997 *Journal of Fluid Mechanics* **338**, 387–410. On the behaviour of a fluid-loaded cylindrical shell with mean flow.
14. R. J. LINGWOOD and N. PEAKE 1998 *Journal of Fluid Mechanics* **396**, 319–344. On the causal behaviour of flow over a compliant wall.
15. L. RAYLEIGH 1945 *The Theory of Sound*, Vols. I and II. New York: Dover.
16. M. J. LIGHTHILL 1960 *Philosophical Transactions of the Royal Society of London* **252**, 397–430. Studies on magnetohydrodynamic waves and other anisotropic wave motions.
17. T. B. BENJAMIN 1963 *Journal of Fluid Mechanics* **16**, 436–450. The threefold classification of unstable disturbances in flexible surfaces bounding inviscid flows.
18. M. T. LANDAHL 1962 *Journal of Fluid Mechanics* **13**, 609–632. On the stability of a laminar incompressible boundary layer over a flexible surface.
19. R. A. CAIRNS 1979 *Journal of Fluid Mechanics* **92**, 1–14. The role of negative energy waves in some instabilities of parallel flows.